Printable High-Aspect Ratio and High-Resolution Cu Grid Flexible Transparent Conductive Film with Figure of Merit over 80 000

Xiaolian Chen, Shuhong Nie, Wenrui Guo, Fei Fei, Wenming Su,* Weibing Gu, and Zheng Cui*

Figure of merit (FOM), the ratio of electrical conductance to optical transparency, is an important metric to evaluate transparent conductive film (TCF). The conductivity of commonly used flexible TCF such as indium tin oxide is generally limited and their FOM is lower than 300. In this study, a high-performance copper (Cu) metal-mesh TCF with the highest FOM ever reported, up to 8×10^4, is fabricated through an additive manufacturing process of blading a silver seed layer and selective electroplating of Cu. With this strategy, Cu metallic lines completely constrained in roll-to-roll imprinted microgrooves achieve high aspect ratio of 2 with 4 µm width and 8 µm depth, which has very clean and smooth edges. This embedded Cu metal mesh exhibits an ultralow sheet resistance down to 0.03 Ω □$^{-1}$ at 86% optical transmittance. It is demonstrated that the Cu metal mesh has remarkable mechanical flexibility, high environmental stability at high temperature and humidity, and durability over repeated heating cycles. The Cu metal mesh is employed as a flexible transparent heater to attach to the windshield of a car, showing rapid heating at low voltage and effective removal of snow.

1. Introduction

Owing to the superior advantages of high transmittance and high conductivity, transparent conductive film (TCF) plays an indispensable role in numerous devices, such as solar cells, display, heating film, and batteries.[1–5] So far, transparent conductive metal-oxides, particularly indium tin oxide (ITO), are predominant in these applications.[6,7] Unfortunately, deposition of ITO requires a high cost vacuum sputtering process.[8,9] ITO is also brittle and not favorable as flexible devices.[3,10]

Dr. X. Chen, S. Nie, W. Guo, F. Fei, Prof. W. Su, Dr. W. Gu, Prof. Z. Cui
Printable Electronics Research Center
Suzhou Institute of Nano-Tech and Nano-Bionics
Chinese Academy of Sciences
Suzhou 215123, China
E-mail: wmsu2008@sinano.ac.cn; zcui2009@sinano.ac.cn
Dr. X. Chen
School of Nano-Tech and Nano-Bionics
University of Science and Technology of China
Hefei 230026, China

The ORCID identification number(s) for the author(s) of this article can be found under https://doi.org/10.1002/aelm.201800991.

To meet the ever increasing requirements of flexible devices, a large number of ITO replacement technologies are emerging, such as carbon nanotubes,[11,12] graphene,[13–16] and metal nanowires (NWs).[17–19] Those carbon-based nanosheets and NWs are famous for the excellent mechanical flexibility, high conductivity, and optical transmittance. However, the thickness of the carbon materials and metal NWs deposited on transparent flexible substrate strongly affects the conductivity and transmittance. Namely, the conductivity increases with the increase of the graphene and nanowire sheet thickness while the optical transmittance decreases. Besides, when NWs are connected to form a conductive layer, the high contact resistance at wire-to-wire junctions degrades the electrical property of TCF and causes high sheet resistance. While applied for large-area electronic devices, especially optoelectrical devices, the high sheet resistance might induce nonuniform light emission, efficiency reduction, and heat generation.[20,21] Based on those considerations, metal-mesh with patterned microscale metal lines emerged as the most promising candidate for flexible TCF materials because of the continuous metallic materials and junction-free characteristic. What is more, the sheet resistance and optical transmittance can be independently adjusted by changing the metal-mesh pitch, line width, metal thickness, as well as applying metals with different resistivity.

Nowadays, metal-meshes have mainly been formed by the micro and nanofabrication method, such as printing metal nanoparticles or nanowires ink,[22,23] self-assembly metal nanoparticles, and ultraviolet (UV) lithography combined with subsequent wet etching.[8,24] However, screen-printing or inkjet printing methods fabricate wide and visible metallic lines, which is extremely difficult to produce high-resolution features and gain high optical transmittance.[25] Moreover, the thicker metal lines by multiple printing passes would further increase the printed line width, which is challenging to achieve high aspect ratio. In authors' group, there are a few attempts to develop high-resolution metal-meshes with uniform metallic lines and conductivity.[26–28] Ag metal-meshes with less than 1 Ω □$^{-1}$ sheet resistance and 88% transmittance have been fabricated previously by embedding Ag nanoparticles (NPs)

into the roll-to-roll imprinted grooves with 1:1 of depth to width aspect ratio and have been successfully applied to touch panel.[28] Lately, a Ag/Ni metal-mesh fabrication process with less than 3 µm line width was developed and combined with a post polishing process, and extremely smooth metal-mesh TCFs were made, which were applied for quantum-dot light-emitting diodes (QLEDs).[26] Though electroplating can fill up the grooves, Ni is not the best conductive material. The metal-mesh TCF in the previous work had sheet resistance of 2.1 Ω $\square^{-1}$, which was alright as transparent electrode for QLED, but not ideal for other applications such as transparent heaters and flexible printed circuits.

Herein, we presented a high aspect ratio Cu metal-mesh with remarkable transparent conductive properties by using an additional manufacturing process of blading Ag seed layer and selective electroplating of Cu. The continuous metallic Cu lines with 2:1 depth to width aspect ratio (4 µm in width and 8 µm in depth) are completely confined to roll-to-roll imprinted microgrooves, achieving clean and smooth edges. In the microgrooves, the Ag seed layer served only as a seed layer at the bottom was sintered by near-infrared (NIR) light for 4 s. And bulk of embedded conductive material was the selectively electroplated Cu. This manufacturing process provides a feasible strategy for developing flexible printed functional circuits with high fidelity. The Cu metal-mesh has extremely low sheet resistance (R_S) down to 0.03 Ω $\square^{-1}$ and still maintains high transmittance of 86%, which achieves the highest figure of merit (FOM) of all reported transparent conductive films, more than 8×10^4. In addition, the Cu metal-mesh shows outstanding mechanical flexibility after 1000 rolling times and good environmental stability at high temperature and humidity. The Cu metal-mesh evaluated as transparent heaters also exhibits uniform and rapid heating performance at a low operating voltage. And after repetitive heating 1000 cycles, the Cu metal-mesh maintains stable thermal stability similar to its initial performance. As a demonstration, a large-size film (30×47 cm²) has been applied for a car windshield to melt snow, showing the effective removal of snow.

2. Results and Discussion

The fabrication process of flexible Cu metal-mesh is schematically illustrated in **Figure 1**a. The imprinted mesh with line spacing of 320 µm was made by roll-to-roll imprinting on polymer substrate to create microgrooves of 4 µm in width
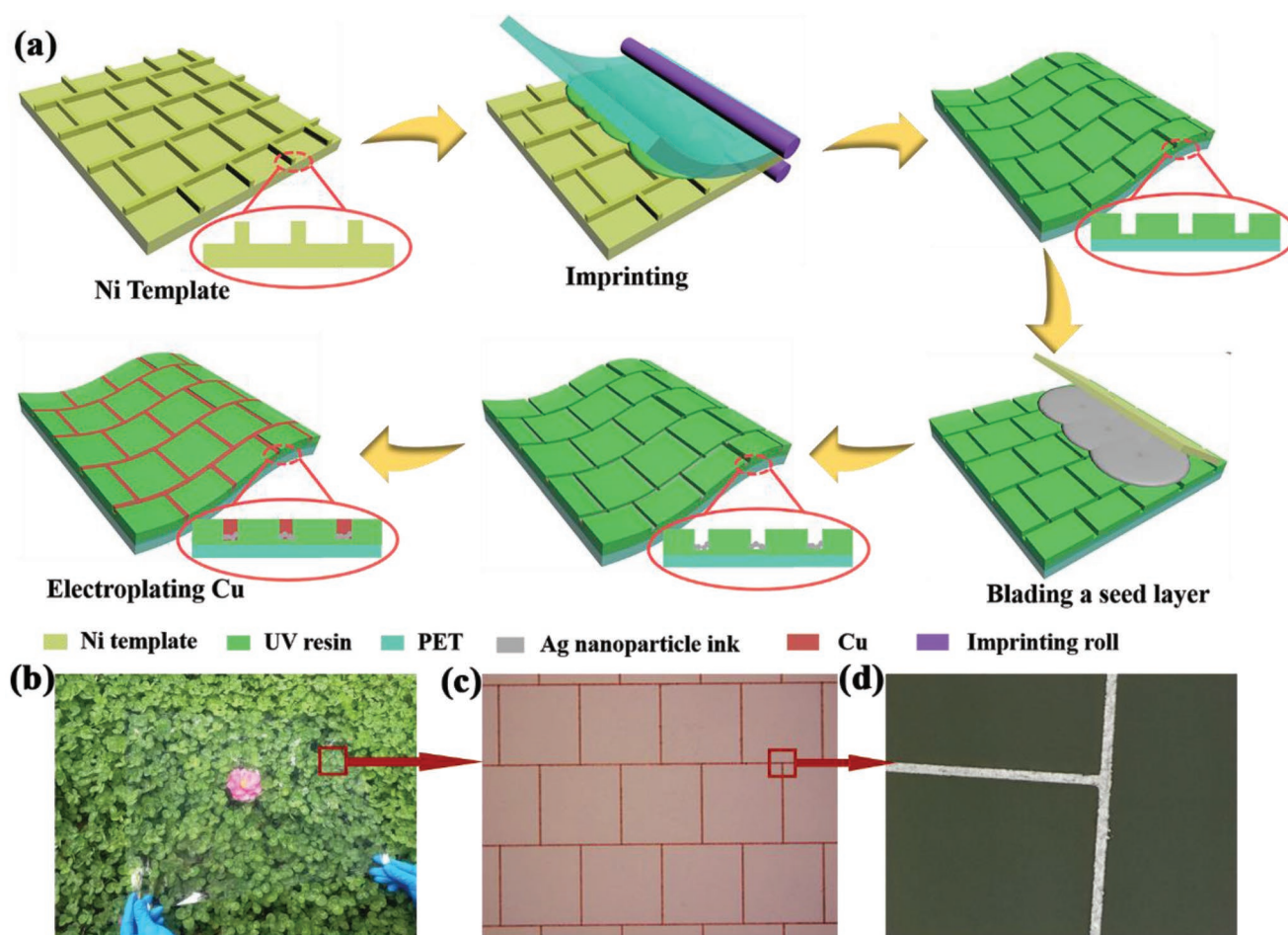

Figure 1. a) Schematics for fabrication process of Cu metal-mesh film; b) Large-size (30×47 cm²) flexible Cu metal-mesh TCF; and c,d) The optical microscopic image.

and 8 µm in depth (2:1 depth to width aspect ratio) (Figure S1, Supporting Information). In the roll-to-roll imprinting process, different patterned structures, such as square, hexagon, rhombus, and random, can also be made with different line width and depth (Figure S2, Supporting Information). That is, different resolution and aspect ratio pattern structures can be produced according to application requirements. Then Ag NP ink with the thickness of 500 nm was filled into the bottom of microgrooves (Figure 2a and Figure S3, Supporting Information). To make a conductive seed layer for Ag NPs, the NIR method was used for 4 s, which is much more effective compared with the traditional heating sintering. Cu electroplating was subsequently performed to fill up the remaining depth of grooves on the top of Ag nanoparticles (Figures S4–S6, Supporting Information). The metallic Cu thickness is adjusted by changing the electroplating time. Furthermore, the different-size Cu metal-mesh film, up to 30×47 cm^2, could be made. Figure 1b shows an example of large-size (30×47 cm^2) flexible Cu metal-mesh film.

Figure 2 shows the progression of electroplating Cu into the microgrooves, from initial only Ag NPs (Figure 2a) to the accumulation of Cu in the grooves after 9, 13, and 18 min of electroplating time (Figure 2b,c). It is observed that more and more metallic Cu was deposited into the microgrooves with increasing electroplating time; the measurements are shown in Figures S4–S6 (Supporting Information). While electroplating for 9 min, the thickness of copper increased from 0 to 4.8 µm and the grooves were partially filled (as seen in Figure 2d). Further plating for 13 min, the copper with the thickness of 8 µm would be fully filled in the grooves (Figure S5, Supporting Information). Even the electroplating copper was completely confined in the microgrooves and the metallic Cu lines had clean and smooth edges, which formed high aspect ratio Cu metal-mesh (2:1 depth to width aspect ratio) (Figure 2e). Compared with screen printing and inkjet printing (typically less than 1 aspect ratio, more than 10 µm line width), this hybrid-printing method has more obvious advantages to obtain much narrower line width and higher aspect ratio. And those excellent features are essential for the application of flexible functional circuits and optoelectronic devices. It is also observed that the electroplated metallic Cu on top of porous Ag NPs is much dense and takes up bulk of embedded conductive material in
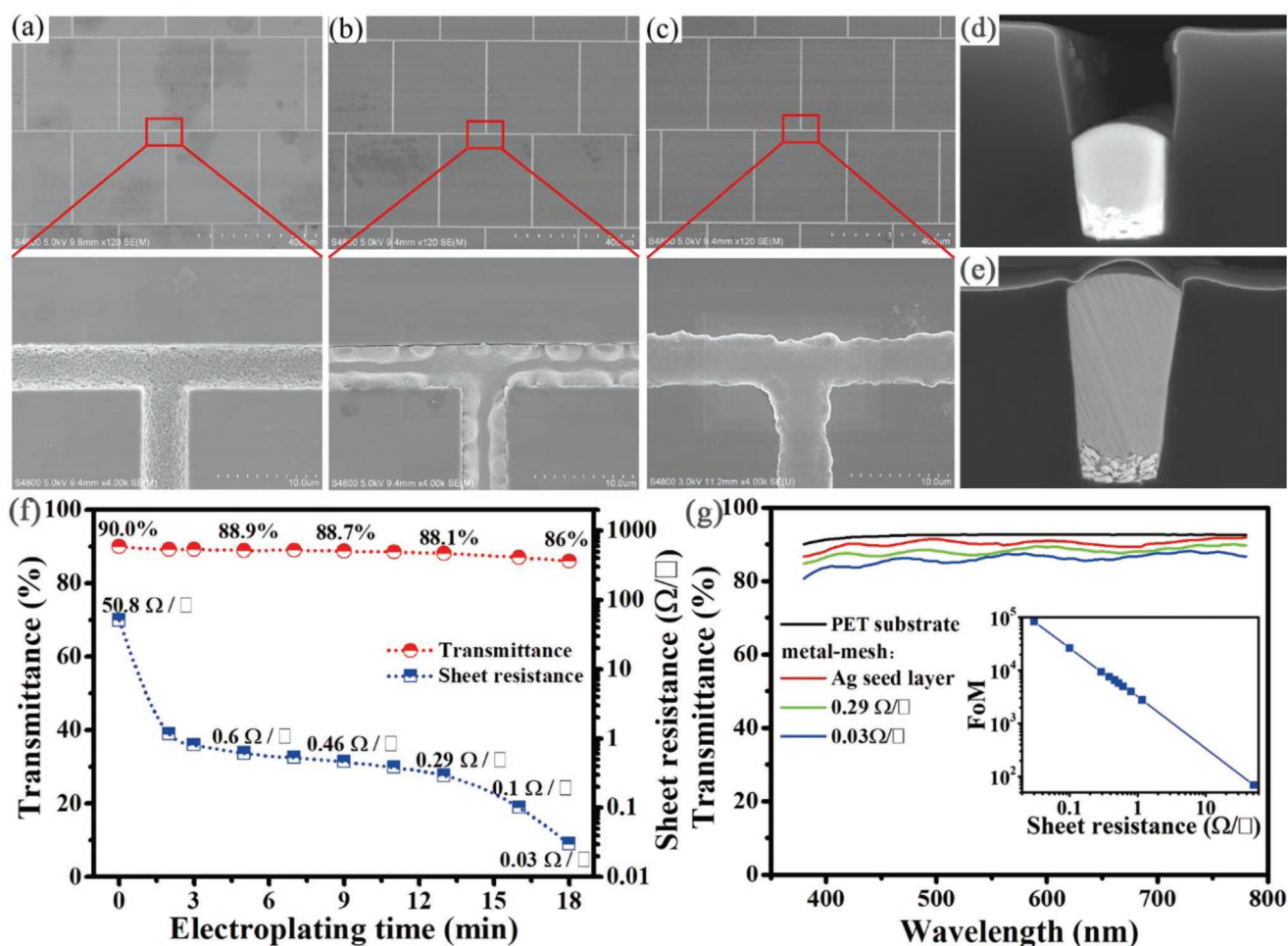
Figure 2. SEM images of Cu metal-mesh at different electroplating time: a) before electroplating; b) 9 min; c) 13 min; the cross-sectional images: d) 9 min and e)13 min; f) Sheet resistance and the average optical transmittance versus different electroplating time; and g) The transmittance of metal-mesh under different conditions and the calculated FOM in the inset.

**ADVANCED
SCIENCE NEWS**
www.advancedsciencenews.com

**ADVANCED
ELECTRONIC
MATERIALS**
www.advelectronicmat.de

Table 1. Comparison of different transparent conductive films reported in literatures with the present work.

Material	Substrate	T[a)] at 550 nm	R_s[b)] [Ω □$^{-1}$]	FOM	Ref.	Method
This work	PET	86.5%	0.03	8.3×10^4		Roll-to-roll imprinting and electroplating Cu
Metal-mesh	Cyclic olefin copolymer	70%	0.07	1.5×10^4	[29]	UV lithography and electroplating Cu
Ionogel/CuG@PET	PET	90%	10.9	320	[31]	UV lithography and electroless deposition of patterned Cu
Cu mesh	Glass	82%	0.2	9035	[32]	UV lithography and electroplating Cu
PEDOT:PSS	PET	87%	57	46	[33]	Spin-coating PEDOT-based materials
Carbon nanotube	PI	77.6%	1169	1.2	[34]	Spray coating carbon nanotubes
Graphene	PET	90%	30	116	[14]	CVD method
Graphene+Ag grid	PET	78%	4	356	[22]	Hot pressing transfer and electrohydrodynamic jet printing
Ag nanofiber networks	Hybrimer resin	91%	3	1301	[35]	Electrospinning Ag nanofibers
Ag nanofiber network	PET	95%	12	605	[36]	Blow spinning and UV irradiation
Ag nanowires	PET	90%	15.6	223	[17]	Drop-coating Ag nanowires
ITO	PET	90%	10	348	[37]	Vacuum deposition

[a)]Transmittance (including the underlying substrate); [b)]Sheet resistance.

the microgrooves, which in turn results in good conductivity close to bulk Cu. However, while increasing the electroplating time, the Cu was spilled over the groove edge and the metal line width began to swell slowly after fully filling grooves, as shown in Figure S6 (Supporting Information). The Cu line swelled to 5.9 µm after 18 min electroplating and Cu protruded 2.8 µm above the substrate surface.

The change about the average optical transmittance at the wavelength range of 380–780 nm and sheet resistance of Cu metal-mesh, from an initial seed layer to the gradual accumulation of Cu in the microgrooves, is presented in Figure 2f. Transmittance of imprinted high aspect ratio mesh structures is about 91.3%, as shown in Figure 2g. The transmittance of fully filled Cu metal-mesh including polyethylene terephthalate (PET) substrate is about 88.1% while 90% for only a Ag seed layer. Therefore, transmittance just changed 2% before fully filling grooves, which is due to the inverted trapezoid cross section of microgrooves causing the subtle change of metallic Cu coverage area (Figure 2e). In parallel, sheet resistance from only a seed layer to fully filling Cu in the microgrooves varied from 50.8 to 0.29 Ω □$^{-1}$. So the sheet resistance of Cu metal-mesh, down up to 0.29 Ω □$^{-1}$, can be randomly adjusted by electroplating the different metallic thickness while the transmittance just changes within 2%. After 18 min electroplating, due to the line width swelling, the sheet resistance is down up to 0.03 Ω □$^{-1}$ and there is a little decrease in the transmittance, keeping 86%. This is the lowest sheet resistance ever reported for a transparent conductive film at the high transmittance of 86%.[14,18,29] Although Cu metal-mesh TCF has a reddish color, which has some disadvantages for practical device applications, a thin nickel layer of about 10–20 nm on top of copper would be electroplated to eliminate the reddish color, as shown in Figure S11 (Supporting Information). Moreover, a thin nickel layer has no influence on the conductivity. Thus, the outstanding optoelectronic properties have a promising application prospect for flexible circuit boards, sensors with high sensitivity, and transparent antenna.

In order to compare comprehensively the optoelectronic properties of Cu metal-mesh with different sheet resistance, a widely used FOM, which is the ratio of electrical conductance to optical comductance, was used to quantitatively compare the TCFs. The relationship between the sheet resistance and transparency was calculated by using the equation below[10,29,30]

$$\text{FOM} = \frac{\sigma_{dc}}{\sigma_{opt}} = \frac{188.5}{R_s * \left(\frac{1}{\sqrt{T}} - 1 \right)}$$

where T is the tranmittance at 550 nm and R_s is the sheet resistance. The inset image in Figure 2g shows the calculated FOMs of Cu metal-mesh, and Cu metal-meshes with 0.03 Ω □$^{-1}$ have much high FOMs, achieving up to 8×10^4, which are among the highest values in recently reported articles. **Table 1** presents a comparison of Cu metal-mesh about optoelectronic properties with other transparent conductive film reported in recent years. Those results clearly demonstrate that Cu metal-mesh in this work has superior overall property compared with other reported materials, such as metal-meshes, nanotubes, graphene, and metal nanowires.

To demonstrate the potential of Cu metal-mesh applied for transparent flexible heater, three 10×2 cm^2 flexible Cu metal-mesh heating strips were fabricated; an example is shown in **Figure 3**a. Although the transparent flexible heater's structure and principle are simple, its high heating performance with a low voltage, high transmittance, and rapid response can be achieved only with a superior transparent conductive film. As shown in Figure 3b, the infrared image of heated strip indicated the heating was very uniform even with the bending. Figure 3c presents the time-dependent temperature rise at different applied voltages for Cu metal-mesh of 0.29 Ω □$^{-1}$. At 2 V of applied voltage, the metal-mesh was heated from 23 to 40 °C in 30 s, while in the same time span at 5 V it was heated to 110 °C. The Cu metal-mesh heater with high sheet resistances also exhibited excellent heating performance (Figure S7, Supporting Information).

Figure 3d compares the saturated temperature as a function of applied voltage for the Cu metal-mesh and commercial ITO with measured sheet resistance of 25 Ω □$^{-1}$. To heat up to 46 °C
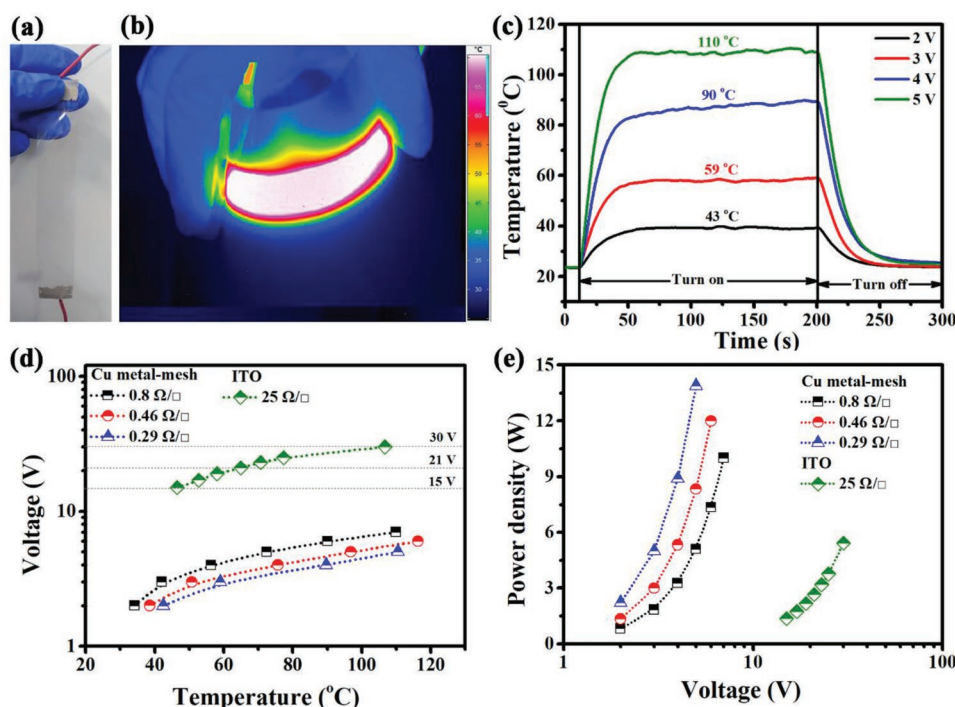
Figure 3. a) Cu metal-mesh heater; b) The infrared picture while bending; c) The temperature profiles of Cu metal-mesh heater (0.29 Ω □$^{-1}$) when applied with different input voltage; d) Saturated temperature as a function of voltage; and e) Power–voltage curves.

with the ITO film, 15 V of voltage was needed and to 113 °C, it would need 30 V (the time-dependent temperatures of ITO film at different applied voltages are shown in Figure S8, Supporting Information). In contrast, Cu metal-mesh films with sheet resistances of 0.29, 0.46, and 0.8 Ω □$^{-1}$ needed only 5–7 V to reach the 110 °C temperature. It is attributed that the joule heating depends on the resistance, which has the relation of $P = U^2/R$ (where P is the heating power, U is the applied bias voltage, and R is the resistance).[4,38] When operated at the constant voltage, the lower resistance is an important factor to maximize desired heating properties. Figure 3e gives the relationship between input power and applied voltage for the two types of film heaters. With applied voltage of 2 V, Cu metal-mesh could generate heating power of 0.816, 1.333, and 2.22 W, whereas the ITO heater required 15 V to generate power of 1.355W. This is mainly due to the much better conductivity of Cu metal-mesh.

The heaters always work in cold or humid condition and their environmental stability is a very important property. The environmental stability of Cu metal-mesh film was evaluated by placing it in a test chamber, which can create high temperature (85 °C) and high relative humidity (85%) conditions. After exposuring 100 h in such conditions, the film showed only less than 10% change of sheet resistance, as shown in **Figure 4**a. This was mainly due to the dense microstructure of electroplated Cu (scanning electron microscopy (SEM) image in Figure 2d,e), which relieved the further oxidation of Cu. The dynamic heating property after exposing to the harsh condition at different lengths of time is shown in Figure 4b. There was only 3% change for the saturated temperature, which was mainly caused by air fluctuations. Moreover, the

uniform heating feature still maintained after 100 h of exposure to the conditions as shown by the infrared image (inset in Figure 4b). This experiment verified that Cu metal-mesh has excellent environmental stability even under extreme conditions.

The mechanical flexibility of Cu metal-mesh was investigated by rolling the films repeatedly around 5 mm radius and measuring the change of their sheet resistance. In comparison to other bending tests, rolling is a much harsh method to test mechanical flexibility.[39] The measurement results up to 1000 rollings are shown in Figure 4c. Only slight variation (within 13%) was observed after 1000 rolling cycles. The uniform heating temperature was maintained (inset infrared picture in Figure 4c). Moreover, the Cu metallic lines are still intactly embedded in the microgrooves (as shown in Figure S9, Supporting Information). The stability of cyclic heating of Cu metal-mesh was investigated by repeated turning on for 150 s and turning off for 100 s at 4 V applied voltage up to 1000 cycles. Figure 4d shows the saturated temperature at 4 V just changed within 3 °C during the 1000 cycles and the heating and cooling properties had no significant changes (Figure 4e,f). Therefore, the Cu metal-mesh exhibits remarkable durability when applied to the windshield heating or other heating elements.

To demonstrate its practical application, the Cu metal-mesh was placed underneath a piece of glass (10 × 10 cm^2 and 0.7 mm thickness), which was covered with a layer of ice (2.5 mm thickness), as shown in **Figure 5**a. By applying 9 V voltage to heat up the underneath Cu metal-mesh film for 3 min, the ice was completely melted into water, as shown in Figure 5b. The dynamic melting process is also provided in Movie S1 (Supporting Information). Another interesting experiment was conducted
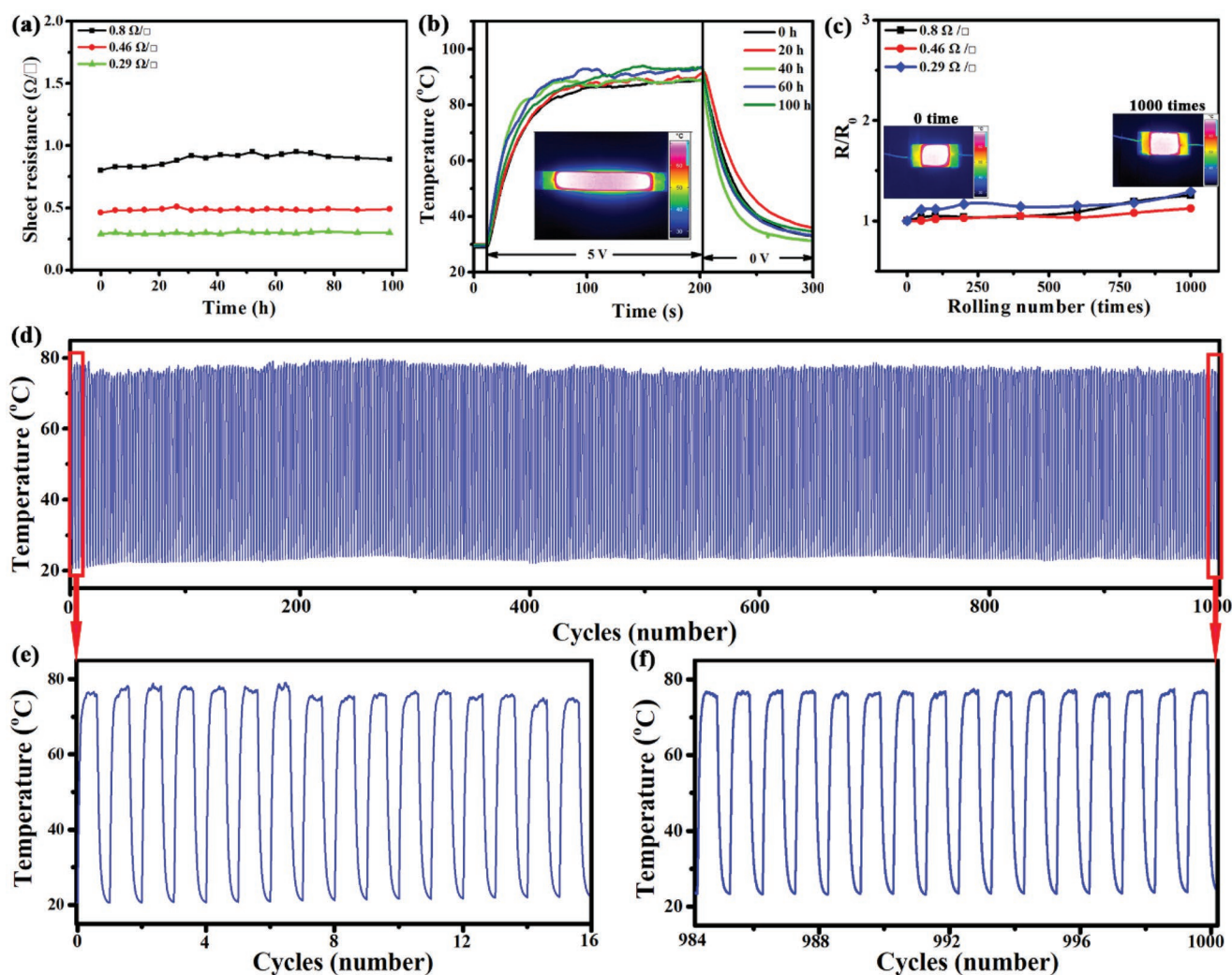
Figure 4. a) R_S variation and b) the heating property of Cu metal-mesh corresponding to the exposure time under high temperature (85 °C) and high relative humidity (85%). Inset: An infrared picture after exposuring 100 h; c) variation of R_S during 1000 cycles of rolling test with the radius of 5 mm. Insets: The infrared pictures after different rolling cycles; and (d–f) Cyclic heating stability versus cyclic numbers.
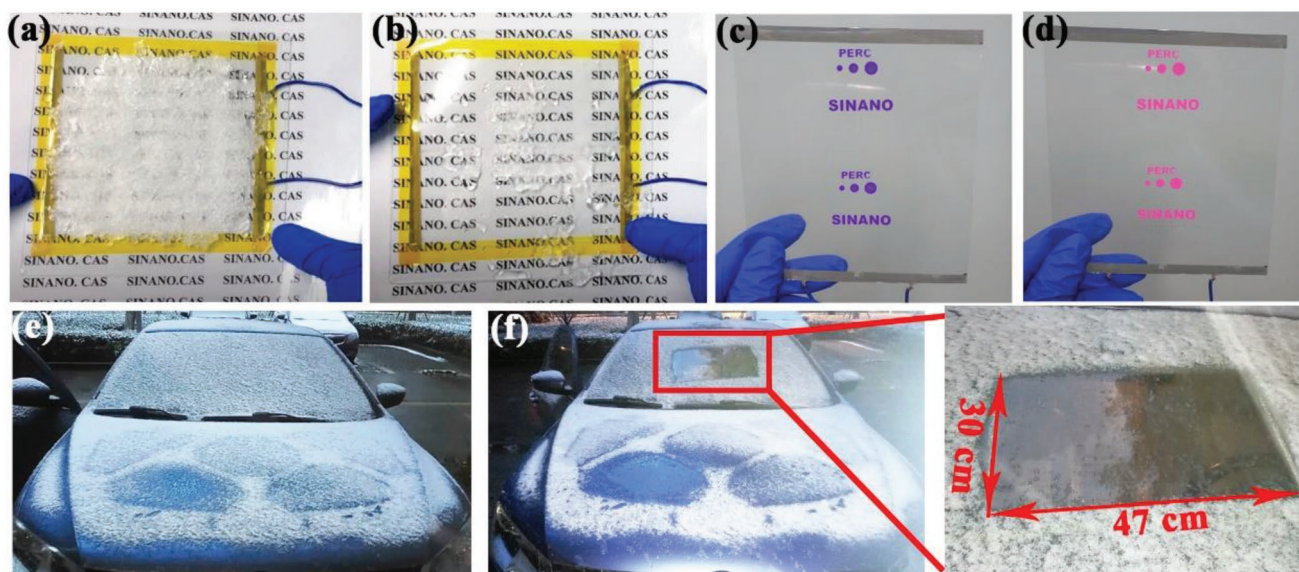
to demonstrate the transparent heating film for thermochromic display. A thermochromic material with an original purple color was screen-printed as characters on the back of Cu metal-mesh (Figure 5c). By applying 5 V voltage to heat up the film to the switching temperature (50 °C) of thermochromic material, the printed characters quickly changed color from purple to pink (Figure 5d).

To prove that the Cu metal-mesh could work as a transparent heating film to deice car windshield, a large-size Cu metal-mesh (30 × 47 cm²) was fabricated. The average sheet resistance was 0.42 Ω □⁻¹, which was determined by measuring 96 different locations over the entire film (detailed data are shown in Figure S10, Supporting Information). On a snowy day, when the windscreen of a car was fully covered with snow flakes (Figure 5e), the Cu metal-mesh was attached to the backside of windshield and applied 20 V voltage. After 5 min, the area where the metal-mesh was attached had snow completely cleared (Figure 5f). A video showing the melting process is also provided in Movie S2 (Supporting Information).

3. Conclusion

In this work, a high aspect ratio and high resolution transparent conductive film has been realized by combining blading Ag seed layer and selectively electroplating of Cu in roll-to-roll imprinted microgrooves. At the microgrooves width of 4 μm, depth of 8 μm, and mesh line spacing of 320 μm, extremely low sheet resistance down to 0.03 Ω □⁻¹ has been achieved while still maintaining high transmittance of 86%, which is believed to be the lowest sheet resistance ever reported for high transparent conductive film in the literature. Tests in harsh environment (85 °C temperature and 85% humidity) proved that the Cu metal-mesh has good environmental stability. The Cu metal-mesh also showed excellence in mechanical flexibility, cyclic heating stability, and heating uniformity across large area. Those outstanding properties proved that the Cu metal-mesh would be robust in many practical applications, such as sensor, heater, and flexible printed circuits. Evaluated as a flexible transparent heater, Cu metal-mesh

ADVANCED
SCIENCE NEWS
www.advancedsciencenews.com

ADVANCED
ELECTRONIC
MATERIALS
www.advelectronicmat.de

Figure 5. a) 10×10 cm^2 glass covered with 2.5 mm thick ice and b) melted into water by heating film; c) Thermochromic display before heating and d) after heating; and e) Car windshield covered with snow f) melted by heating film.

heater presents uniform and effective heating performance. As application demonstrations, deicing experiments have been conducted, showing effectiveness in melting thick ice and in clearing snow covered windshield of a car. Although Cu metal-mesh is presently made in laboratory, the additive manufacturing process can be implemented in industry scale roll-to-roll manufacturing and suitable for many applications, such as optoelectronic devices, sensors, and flexible printed functional circuits.

4. Experimental Section

Preparation of Cu Metal-Mesh: Figure 1a illustrates the fabrication process of Cu metal-mesh, and a nickel (Ni) master was made with patterned microstructures as the imprinted template. The template was imprinted into a layer of UV curing adhesive on PET substrate to form high aspect ratio grooves (Figure S1, Supporting Information). Ag NP ink (Henkel AG & Co. KGaA) was subsequently filled into the microgrooves as an electroplating seed layer. And there were no Ag NP leftovers on the surface of substrate by adjusting the surface tension of Ag NP ink and optimizing blade angle between the blade and substrate. The Ag seed layer was sintered by NIR for 4 s (wavelength rage: 800–1500 nm, 500 W, Heraeus). Then Cu was selectively electroplated on the top of conductive Ag nanoparticles in the microgrooves with the current density of 1.5 A dm^{-2}. The plating Cu solutions were purchased from Sur-Precision Metal Technology Co., LTD. The whole process was performed in ambient condition.

Fabrication of Cu Metal-Mesh Heater: Cu metal-mesh heaters were fabricated using a two-terminal side contact configuration. In order to lower the contact resistance between Cu metal-mesh and the external connection, silver paste was used to fix the external wires on both sides of Cu metal-mesh. The DC power supply (IT6500D, ITECH) was used to obtain joule heating. The temperature of the heaters was monitored using thermistor and infrared images were captured by the infrared camera.

Characterization of Cu Metal-Mesh: The morphology and cross-section of Cu metal-mesh was observed by SEM (Hitachi S-4800). The width and depth of metallic lines in the grooves were characterized by optical microscopy (color 3D laser scanning microscope VK-9710, KEYENCE).

A UV–visible spectrometer (Lambda 750, PerkinElmer) was used to measure the transmittance of Cu metal-mesh, and four-point probe station (Suzhou Jingge Electronic Co., Ltd) was used to characterize R_S at room temperature. Mechanical reliability of Cu metal-mesh was investigated under repeated rolling by a homemade bending tester with rolling diameter of 10 mm. Temperature and humidity test chamber (SXN403, Kusumoto Chemicals, Ltd) was used to characterize oxidation resistance of Cu metal-mesh under the conditions of 85% relative humidity and 85 °C temperature.

Supporting Information

Supporting Information is available from the Wiley Online Library or from the author.

Conflict of Interest

The authors declare no conflict of interest.

Keywords

Cu metal-mesh, high aspect ratio, high resolution, transparent conductive film

ADVANCED
SCIENCE NEWS
www.advancedsciencenews.com

ADVANCED
ELECTRONIC
MATERIALS
www.advelectronicmat.de

[1] J. Wu, X. L. Que, Q. Hu, D. Y. Luo, T. H. Liu, F. Liu, T. P. Russell, R. Zhu, Q. H. Gong, *Adv. Funct. Mater.* **2016**, *26*, 4822.

[2] K. Ellmer, *Nat. Photonics* **2012**, *6*, 809.

[3] J. A. Spechler, T.-W. Koh, J. T. Herb, B. P. Rand, C. B. Arnold, *Adv. Funct. Mater.* **2015**, *25*, 7428.

[4] J. J. Bae, S. C. Lim, G. H. Han, Y. W. Jo, D. L. Doung, E. S. Kim, S. J. Chae, T. Q. Huy, N. V. Luan, Y. H. Lee, *Adv. Funct. Mater.* **2012**, *22*, 4819.

[5] M. V. M. Rao, Y. K. Su, T. S. Huang, Y.-C. Chen, *Nano-Micro Lett.* **2010**, *2*, 242.

[6] R. Gupta, K. D. M. Rao, S. Kiruthika, G. U. Kulkarni, *ACS Appl. Mater. Interfaces* **2016**, *8*, 12559.

[7] B. D. Choi, J. Park, K. J. Baeg, M. Kang, J. S. Heo, S. Kim, J. Won, S. Yu, K. Ahn, T. H. Lee, J. Hong, D. Y. Kim, H. Usta, C. Kim, S. K. Park, M. G. Kim, *Adv. Electron. Mater.* **2018**, *4*, 11.

[8] L. Zhou, M. Yu, X. Chen, S. Nie, W.-Y. Lai, W. Su, Z. Cui, W. Huang, *Adv. Funct. Mater.* **2018**, *28*, 1705955.

[9] S. Ye, A. R. Rathmell, Z. Chen, I. E. Stewart, B. J. Wiley, *Adv. Mater.* **2014**, *26*, 6670.

[10] B. Han, K. Pei, Y. Huang, X. Zhang, Q. Rong, Q. Lin, Y. Guo, T. Sun, C. Guo, D. Carnahan, M. Giersig, Y. Wang, J. Gao, Z. Ren, K. Kempa, *Adv. Mater.* **2014**, *26*, 873.

[11] Y. H. Yoon, J. W. Song, D. Kim, J. Kim, J. K. Park, S. K. Oh, C. S. Han, *Adv. Mater.* **2007**, *19*, 4284.

[12] Z. Wu, Z. Chen, X. Du, J. M. Logan, J. Sippel, M. Nikolou, K. Kamaras, J. R. Reynolds, D. B. Tanner, A. F. Hebard, A. G. Rinzler, *Science* **2004**, *305*, 1273.

[13] Z. Pei, H. Hu, G. Liang, C. Ye, *Nano-Micro Lett.* **2016**, *9*, 19.

[14] S. Bae, H. Kim, Y. Lee, X. F. Xu, J. S. Park, Y. Zheng, J. Balakrishnan, T. Lei, H. R. Kim, Y. I. Song, Y. J. Kim, K. S. Kim, B. Ozyilmaz, J. H. Ahn, B. H. Hong, S. Iijima, *Nat. Nanotechnol.* **2010**, *5*, 574.

[15] J. Ning, L. Hao, M. Jin, X. Qiu, Y. Shen, J. Liang, X. Zhang, B. Wang, X. Li, L. Zhi, *Adv. Mater.* **2017**, *29*, 1605028.

[16] J. Kang, H. Kim, K. S. Kim, S.-K. Lee, S. Bae, J.-H. Ahn, Y.-J. Kim, J.-B. Choi, B. H. Hong, *Nano Lett.* **2011**, *11*, 5154.

[17] J. Wang, J. Jiu, T. Araki, M. Nogi, T. Sugahara, S. Nagao, H. Koga, P. He, K. Suganuma, *Nano- Micro Lett.* **2014**, *7*, 51.

[18] Z. Zhong, H. Lee, D. Kang, S. Kwon, Y. M. Choi, I. Kim, K. Y. Kim, Y. Lee, K. Woo, J. Moon, *ACS Nano* **2016**, *10*, 7847.

[19] S. Hong, H. Lee, J. Lee, J. Kwon, S. Han, Y. D. Suh, H. Cho, J. Shin, J. Yeo, S. H. Ko, *Adv. Mater.* **2015**, *27*, 4744.

[20] Y. Galagan, E. W. C. Coenen, W. J. H. Verhees, R. Andriessen, *J. Mater. Chem. A* **2016**, *4*, 5700.

[21] H. Tang, Y. Jiang, C. W. Tang, H.-S. Kwok, *J. Disp. Technol.* **2016**, *12*, 605.

[22] J. Kang, Y. Jang, Y. Kim, S. H. Cho, J. Suhr, B. H. Hong, J. B. Choi, D. Byun, *Nanoscale* **2015**, *7*, 6567.

[23] L. Li, M. Gao, Y. Guo, J. Sun, Y. Li, F. Li, Y. Song, Y. Li, *J. Mater. Chem. C* **2017**, *5*, 2800.

[24] a) Y. D. Suh, J. Kwon, J. Lee, H. Lee, S. Jeong, D. Kim, H. Cho, J. Yeo, S. H. Ko, *Adv. Electron. Mater.* **2016**, *2*, 1600277; b) K.-W. Seo, Y.-J. Noh, S.-I. Na, H.-K. Kim, *Sol. Energy Mater. Sol. Cells* **2016**, *155*, 51; c) S. Bai, S. Zhang, W. Zhou, D. Ma, Y. Ma, P. Joshi, A. Hu, *Nano-Micro Lett.* **2017**, *9*, 42.

[25] T. Zhang, X. Wang, T. Li, Q. Guo, J. Yang, *J. Mater. Chem. C* **2014**, *2*, 286.

[26] X. Chen, W. Guo, L. Xie, C. Wei, J. Zhuang, W. Su, Z. Cui, *ACS Appl. Mater. Interfaces* **2017**, *9*, 37048.

[27] X. L. Chen, X. Z. Wu, S. S. Shao, J. Y. Zhuang, L. M. Xie, S. H. Nie, W. M. Su, Z. Chen, Z. Cui, *Sci. Rep.* **2017**, *7*, 13239.

[28] Z. Cui, Y. Gao, *Dig. Tech. Pap.—Soc. Inf. Disp. Int. Symp.* **2015**, *46*, 398.

[29] A. Khan, S. Lee, T. Jang, Z. Xiong, C. Zhang, J. Tang, L. J. Guo, W. D. Li, *Small* **2016**, *12*, 3021.

[30] M. Vosgueritchian, D. J. Lipomi, Z. Bao, *Adv. Funct. Mater.* **2012**, *22*, 421.

[31] L. Chang, X. Zhang, Y. Ding, H. Liu, M. Liu, L. Jiang, *ACS Appl. Mater. Interfaces* **2018**, *10*, 29010.

[32] S. Shen, S.-Y. Chen, D.-Y. Zhang, Y.-H. Liu, *Opt. Express* **2018**, *26*, 21.

[33] M. N. Gueye, A. Carella, R. Demadrille, J. P. Simonato, *ACS Appl. Mater. Interfaces* **2017**, *9*, 27250.

[34] S. K. Kim, T. Liu, X. Wang, *ACS Appl. Mater. Interfaces* **2015**, *7*, 20865.

[35] J. Park, B. G. Hyun, B. W. An, H. G. Im, Y. G. Park, J. Jang, J. U. Park, B. S. Bae, *ACS Appl. Mater. Interfaces* **2017**, *9*, 20299.

[36] S. Lin, X. P. Bai, H. Y. Wang, H. L. Wang, J. N. Song, K. Huang, C. Wang, N. Wang, B. Li, M. Lei, H. Wu, *Adv. Mater.* **2017**, *29*, 7.

[37] R. Bel Hadj Tahar, T. Ban, Y. Ohya, Y. Takahashi, *J. Appl. Phys.* **1998**, *83*, 2631.

[38] a) S. Ji, W. He, K. Wang, Y. Ran, C. Ye, *Small* **2014**, *10*, 4951; b) H. T. Zhai, R. R. Wang, X. Wang, Y. Cheng, L. J. Shi, J. Sun, *Nano Res.* **2016**, *9*, 3924.

[39] X. Z. Wu, S. S. Shao, Z. Chen, Z. Cui, *Nanotechnology* **2017**, *28*, 035203.